ETH Library

The effect of work function during electron spectroscopy measurements in Scanning Field-Emission Microscopy

Journal Article

Author(s):
Bodik, Michal; Walker, Christopher; Demydenko, Maksym; Demydenko, Maksym; Bähler, Thomas; Ramsperger, Urs; Thamm, Ann-Katrin; Tear, Steve; Pratt, Andrew; El-Gomati, Mohamed; Pescia, Danilo

Publication date:
2022-08

Permanent link:
https://doi.org/10.3929/ethz-b-000547750

Rights / license:
Creative Commons Attribution 4.0 International

Originally published in:
Ultramicroscopy 238, https://doi.org/10.1016/j.ultramic.2022.113547

Funding acknowledgement:
606988 - Sources, Interaction with Matter, Detection and Analysis of Low Energy Electrons 2 (EC)

This page was generated automatically upon download from the ETH Zurich Research Collection.
For more information, please consult the Terms of use.

Ultramicroscopy 238 (2022) 113547

Contents lists available at ScienceDirect

Ultramicroscopy

journal homepage: www.elsevier.com/locate/ultramic

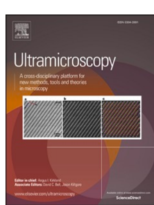

The effect of work function during electron spectroscopy measurements in Scanning Field-Emission Microscopy

Michal Bodik [a,*], Christopher Walker [a], Maksym Demydenko [a], Thomas Michlmayr [a], Thomas Bähler [a], Urs Ramsperger [a], Ann-Katrin Thamm [a], Steve Tear [b], Andrew Pratt [b], Mohamed El-Gomati [c,d], Danilo Pescia [a]

[a] Laboratorium für Festkörperphysik, ETH Zürich, Zürich CH-8093, Switzerland
[b] Department of Physics, University of York, Heslington, York YO10 5DD, United Kingdom
[c] Department of Electronic Engineering, University of York, Heslington, York YO10 5DD, United Kingdom
[d] York Probe Sources Ltd., 7 Harwood Rd, York YO26 6QU, United Kingdom

ARTICLE INFO

Keywords:
Scanning probe energy loss spectroscopy
Miniature electron energy analyser
Scanning tunnelling microscopy
Scanning Field Emission Microscopy

ABSTRACT

Electron spectroscopy proves to be a handy tool in material science. Combination of electron spectroscopy and scanning probe microscopy is possible through Scanning Field Emission Microscopy (SFEM), where a metallic probe positioned close to the surface is used as an electron source. However, using this not too much technologically demanding technique, it looks like the compromise between the lateral resolution and spectroscopic clarity must be considered. Here, we demonstrate, using experimental and simulation data, that the spectroscopic information can be understood without the need to grossly deteriorate the potential spatial resolution of the microscope. We prepared a three-section sample with clean W(110), sub-monolayer Cs on W(110) and monolayer of Cs on W(110) on which electron energy loss spectra are obtained via Scanning Probe Energy Loss Spectroscopy (SPELS) measurements. To explain the detected spectra a new model describing SPELS measurements in a SFEM is developed which aids to uncover the origin of spectral features typically detected during experiments. Experimental and simulation data are in a mutual agreement and observed spectral features on different surfaces could be explained. This novel understanding of SPELS can solve the main issue previously related to this technique, and good spatial resolution can be accompanied by the understanding of the measured spectra.

1. Introduction

Scanning Field-Emission Microscopy (SFEM) is an electron microscopy technique derived from Scanning Tunnelling Microscopy (STM). During STM, the tip is typically approached to the sample at the nanometer range distance with a low tip-sample voltage applied (typically in the order of volts), and the quantum tunnelling effect allows electrons to tunnel between tip and sample, thus creating a current. The surface topography is reconstructed by imaging the electron cloud of the sample surface under the tip. In SFEM, the tip is retracted from the sample up to hundreds of nanometres, and a higher negative voltage is applied to the tip, typically tens to few hundreds of volts. The electron beam can raster the sample by simply moving the tip, and no electron lens system is required.

On top of that, unlike STM, there is a new quantity to measure. Similar to STM, the current between the tip and sample can be measured, but also a current of reflected and absorbed electrons originated from electrons emitted from the tip via field electron emission which impinge the sample surface. The reflected electrons in this set-up can be used for imaging, and it was shown that using this technique, spatial resolution of ~1 nm and 30% contrast between W(110) and ≈0.34 layers of Fe on top of it can be achieved [1].

Another benefit in this arrangement is that sample information can be obtained by the analysis of the surface reflected electrons using electron spectroscopy along with information of surface topography. This technique, which is called Scanning Probe Energy Loss

Abbreviations: SFEM, Scanning Field-Emission Microscopy; SPELS, Scanning Probe Energy Loss Spectroscopy; STM, Scanning Tunneling Microscopy; BBX, Bessel Box; CLAM, Combined Lens and Analyzer Module 2; ML, Monolayer; EELS, Electron Energy Loss Spectroscopy; EEA, Electron Energy Analyser.

* Corresponding author.
E-mail address: mbodik@ethz.ch (M. Bodik).

https://doi.org/10.1016/j.ultramic.2022.113547
Received 15 December 2021; Received in revised form 22 March 2022; Accepted 4 May 2022
Available online 6 May 2022
0304-3991/© 2022 The Author(s). Published by Elsevier B.V. This is an open access article under the CC BY license (http://creativecommons.org/licenses/by/4.0/).

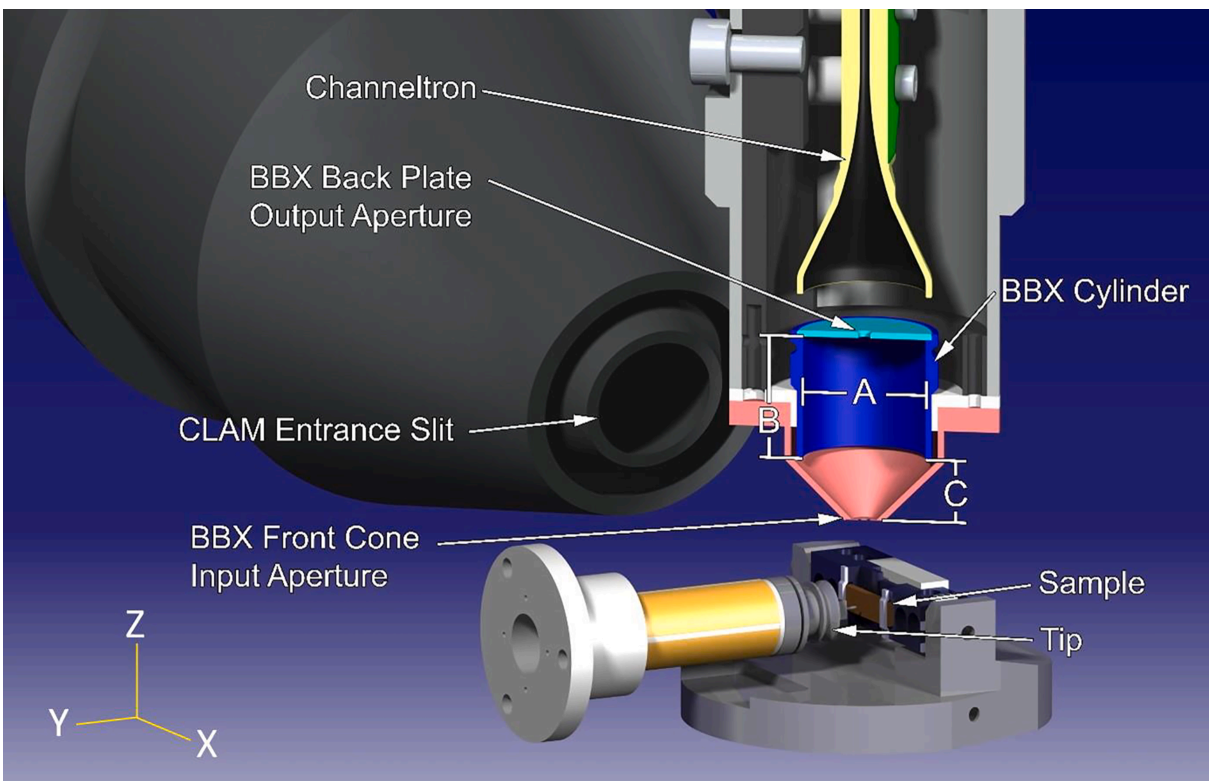

Fig. 1. Schematic design of the configuration inside of the measurement chamber.

Spectroscopy (SPELS), requires an additional electron energy analyser. The spatial resolution of SPELS in the proposed configuration is expected to be similar to that of SFEM [2]. Spatial resolution of 50 nm [3] and energy resolution of about 0.6 eV [2] have already been demonstrated for conventional SPELS. Spectra obtained from graphite and silicon show expected features such as plasmon peaks [4].

During SFEM, the electric field from the tip affects the reflected electrons, effectively pushing them back into the sample [5]. Because of this effect, the tip is typically retracted up to microns or even millimetres above the sample for SPELS measurements, otherwise the spectrum starts to lose its spectral features [6]. However, retracting the tip inevitably results in decreased spatial resolution. Therefore, there must either be a compromise between the spatial resolution and the quality of spectra, or alternatively the spatial resolution is kept as a priority, and obtained spectra can be explained in another manner than "classical" electron energy loss spectroscopy (EELS).

Werner et al. conducted a simulations study, to explain the signal generated for a tip 20 nm away from the sample [5]. From the simulations, these authors concluded two main results. First, the detected signal is made up of back-reflected electrons rather than just secondary electrons. Second, the slow secondary electrons, which are generated by the impinging field emitted electrons from the tip, are pushed back into the sample by an electric field originating from the tip, where they are finally collected some distance away, measuring up to mm away from the point of generation. This means that the detected secondary electrons are not originating from under the tip. Along with these two main conclusions, the authors stated that the material's work function should play only a minor role in the observed spectra.

In the present study, we also examined the effect of work function on SPELS and the results obtained were in contradiction with those by Werner et al. [5] Because of the different results obtained to those of Werner et al.'s simulation and the close proximity of the tip to the sample, we propose a new simulation model. In classical mechanics at the interface of two materials, a part of an incident wave is reflected. The amplitude of the reflected wave is dependent on a difference between refraction indexes. In quantum mechanics, an electron propagates through space as a wave described by its wavefunction. Therefore at the material interface, a part of the wavefunction is reflected back. This results in a non-zero probability in a reflection of an electron from the vacuum-sample interface. An electron can make more than one of such quantomechanical reflections and propagate along sample's surface without entering the material. In our new model we proposed such a mechanism of quantomechanical reflection of electrons [7]. Furthermore, our simulation model and experiment take into account the collection of the reflected electrons by a miniature electron energy analyser in order to investigate the effect of the sample's work function. The proposed model thus enables one to simulate the SPELS experiment in this configuration more accurately as well as shedding some light on other results reported by Werner et al.

Alkali metals are well known for their low work function and are often used to decrease surfaces' work function. Chou et al. proposed an orbital-overlap model that explains the formation of work function minimum during cesiation of metal surfaces [8]. From their work, it is possible to estimate the work function of the surface from the surface coverage. In our experiments, we used Cs deposited on W(110) as a model surface and calculated the work function from their model.

2. Experimental

The homemade ultra-high vacuum (base pressure 4×10^{-11} mbar) STM was equipped with two electron energy analysers (Fig. 1). One was a standard hemispherical Combined Lens and Analyzer Module 2 of VG MICROTECH (CLAM) that was located approximately 40 mm from the tip (Fig. 1). The second electron energy analyser was called the Bessel Box (BBX), which is a miniature electron energy analyser [9] which can be positioned as close as a distance of 2 mm from the tip.

The sample was a single crystal W(110) with a deposited thin film of Cs. Initially the W(110) sample was cleaned by a well-known procedure in the preparation chamber (base pressure $\sim 10^{-10}$ mbar). Annealing in the oxygen atmosphere (partial pressure of $O_2 \sim 4 \times 10^{-8}$ mbar) up to

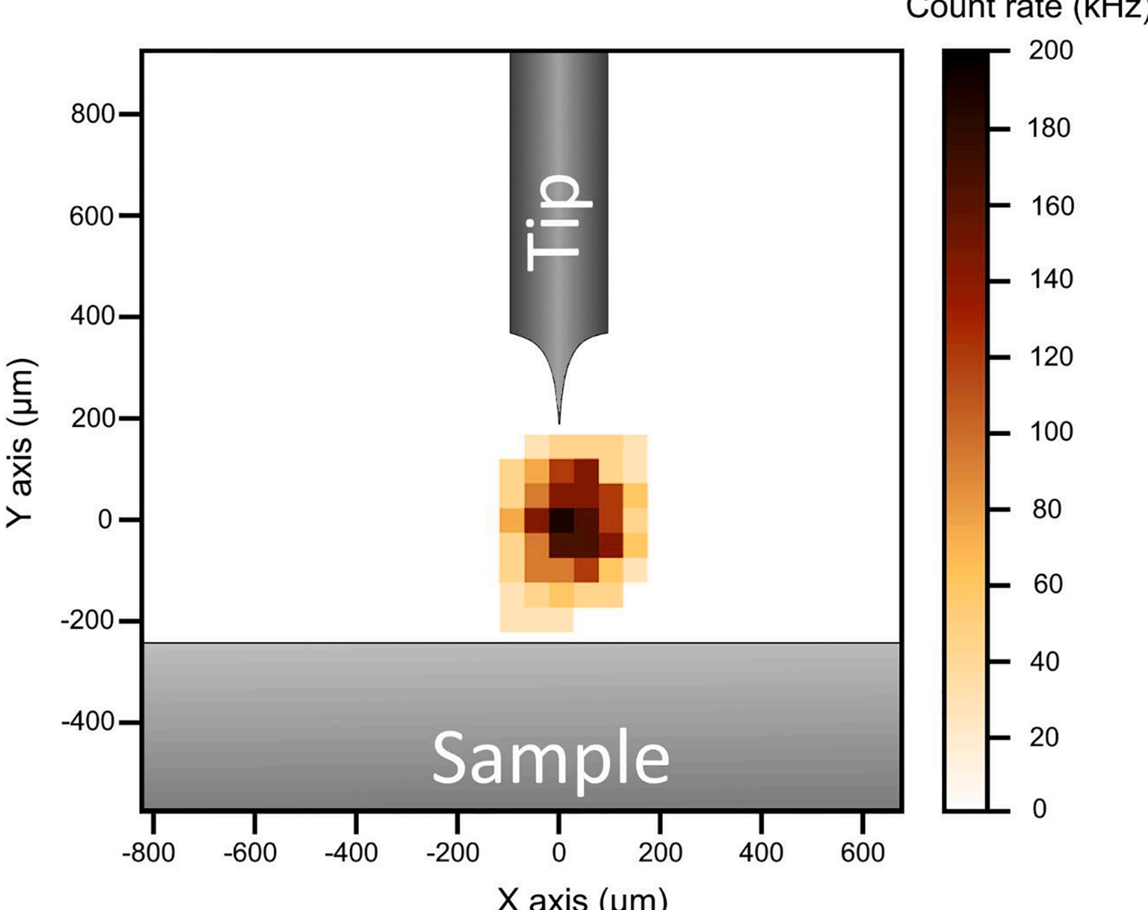

Fig. 2. Intensity distribution based on the BBX position. Note that the distance between the emitter's tip and the sample surface is 200 nm, hence this is in effect the 0,0 points defining the scanned area. This is drawn for illustration purposes only, whilst the BBX movement has a µm scale as shown in the figure.

1400°C followed by a flash annealing up to 2000°C. After the cleaning procedure, a thin film of Cs is evaporated onto the W surface. The Cs source (SAES group, Italy) was heated by DC at 6.5 A. After the deposition current was reached the shutter stayed closed for 5 min, thus letting the Cs flow get more stable. After the flow stabilisation period the shutter in front of the sample was opened to deposit Cs on 1/3 of the W (110) clean surface. After 30 min deposition, the shutter was opened to expose 2/3 of the sample for the deposition for an additional 30 min. This two-step deposition process creates a sample containing three regions; clean W(110), sub-monolayer film of Cs, and a monolayer film of Cs.

The tip was prepared by standard electrochemical etching of cylindrical polycrystalline W wire in NaOH and cleaned *in-situ* in the chamber similar to the sample [10]. A W wire was immersed into 5 mM NaOH solution through the middle of a circular electrode. The wire was immersed in a way, that approximately 4 mm are fully immersed in the etching solution. A constant voltage of 3 V was applied until the wire broke and the immersed part fell off. The cut-off resistance was set to 1.7 kΩ. The *in-situ* cleaning procedure was performed as follows. The tip was placed 4 mm from a heating coil. The current in the heating coil was set to 1.71 A, while the tip was kept at 1000 V. Electrons emitted from the heating coil were bombarding the tip and thus created a current of 4.9 mA flowing in the tip for 5 minutes. Afterwards, 4×10^{-8} mbar of O_2 was introduced into the preparation chamber. In such oxygen atmosphere, the tip was again set to 1000 V and the heating coil was set to 1.72 A. The current of emitted electrons flowing in the tip was 5.0 mA and was kept for 10 minutes. Four short 20 seconds long flashes were performed after the O_2 inlet was closed and the pressure inside the chamber stabilised at $\sim 10^{-10}$ mbar. The tip was kept at 1000 V and the heating coil current was set to 1.84 A, 1.87 A and another 1.84 A twice again. The current in the tip was 15.3 mA, 19.2 mA, 15.6 mA and 15.5 mA respectively. After the cleaning procedure, the tip was mounted into the STM.

The SPELS experiment was performed as follows. First, STM images at all three areas of the sample were measured to confirm the surface coverage. The STM was measured in a constant current mode, with tip voltage at -2 V and sample current of 0.2 nA. After all three STM images were obtained, electron energy loss spectra were measured with the CLAM and BBX electron energy analysers.

The BBX was first aligned by moving it in both the x-axis (parallel to the sample surface) and the y-axis (perpendicular to the sample surface), until the maximum intensity of the elastic peak was found. The intensity distribution with respect to the BBX position is shown in Fig. 2. The position of the sample and the tip as a top view of the BBX schematically shown on the plot, where the zero point is determined by the position for max count found by BBX. Away from it in both x- and y-directions establishes the field of view for the BBX. The BBX alignment was performed at the energy of the elastic peak. The front cone electrode of the BBX was grounded during the measurements.

Before each measurement, the tip was set-up to the tunnelling mode as for standard STM measurements. This position was set as the "zero" position of the tip in order to determine the tip-sample distance later on. The tip was then withdrawn from the zero position by a piezo tube to a distance of 200 nm above the sample surface. The tip voltage was set to -30 V, and a field-emission current of ~200 nA was obtained. The spectra obtained by BBX and presented here are an average of 6

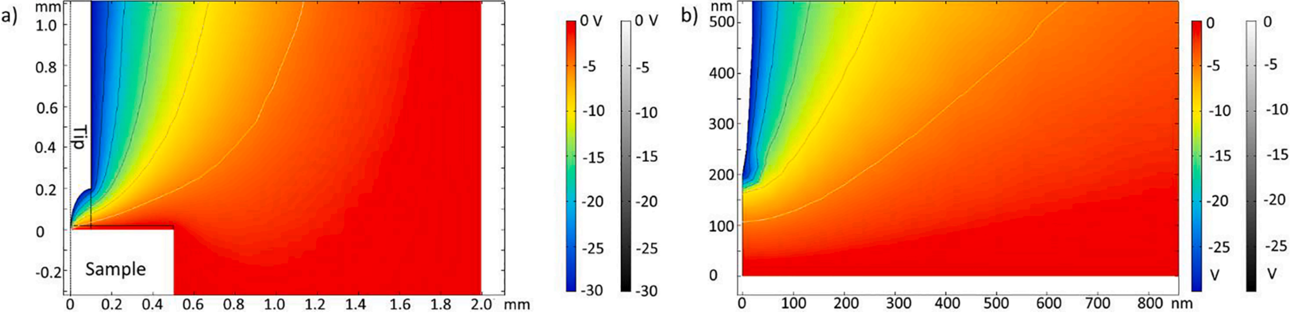

Fig. 3. Cross-sections of the electric field used in the COMSOL Multiphysics simulation. a) The region between sample and detector, and b) Close up of the tip region with contour levels. Regions inside conducting regions are shown as white, the grey dotted line is an axis of rotational symmetry. Certain horizontal and vertical black lines are different regions with different meshing density used in the COMSOL program.

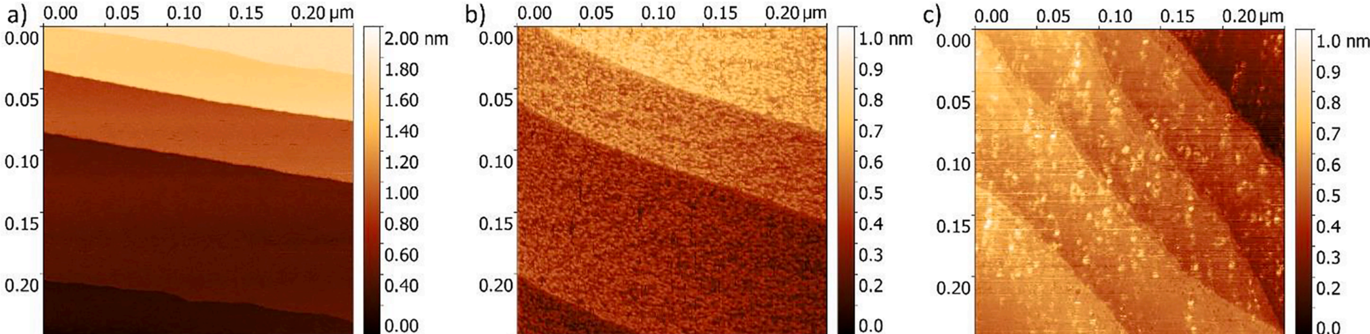

Fig. 4. STM images of a) clean W(110), b) 30 min of Cs deposition, and c) 60 min of Cs deposition. All the scans are 250 × 250 nm^2 and the false colours represent the measured height.

individual measurements, whilst the CLAM spectra are an average of 2 measurements. The measured spectra from both analysers were also normalized to the current absorbed by the sample. This way, the artefacts that originated in the emitted current fluctuations, typical of cold field emission, were reduced.

To confirm the electrons' origin measurements (i.e. those leaving the sample), we observed spectra measured with BBX moved to different x-axis positions. First, the alignment procedure was performed as before and BBX position with the maximised intensity of signal was found. Afterwards, BBX was moved along x-axis by 175 μm, 275 μm and 475 μm without moving the tip and three additional spectra were recorded at those positions. Because the BBX collects electrons from only a limited area from underneath it (i.e. a small field of view), this way we can distinguish which electrons (i.e. with which energy) are leaving the sample from under the tip and which from further away.

To simulate the electric field of the experimental configuration, the COMSOL Multiphysics® v 5.6 (COMSOL AB, Sweden) simulation program has been used. The simulated geometrical structure is shown in Fig. 3.

A 2D axisymmetric electric field was generated using a single mesh structure with very fine detail near to the tip and becoming gradually coarser away from the tip and away from the sample surface. The electric field was swept around the tip to generate an axisymmetric 3D field in which the electron trajectory simulations took place. This was similar to the set-up of Werner et al. [5]. The electron trajectories in the vacuum were simulated using COMSOL, and the electron trajectories in the sample material were simulated using a Monte Carlo (MC) model program [11,12]. Matlab scripts were used to convert the output files from the MC model to the COMSOL format and vice versa. The first part of the procedure was to run the MC simulation. The electrons were launched from directly under the tip vertically downwards. Then take the electrons that had escaped from the surface during the MC simulation and pass these on to the COMSOL program. During their flight in vacuum, the electric field from the tip forced these electrons back onto the surface, so they were again passed back to the MC program. This procedure continues until all electrons had either dissipated all of their energy or were collected at the hypothetical position of the detector. In this configuration, this was the location of the grounded electrode of the electron energy analyser. The effect of quantum mechanical electron skipping at the surface [13] were taken care of in the COMSOL program. For each simulation run 10^6 primary electrons were used, with tip-sample distance of 200 nm, 30 eV electron energy, 2 mm tip-detector distance and 0 V detector bias and sample radius of 0.5 mm.

3. Results and discussion

STM images were obtained on each of the three parts of the sample (Fig. 4). The clean part of the W(110) shows typical flat atomic steps (Fig. 4a). The thickness of deposited Cs layer was calculated from STM measurements. With a 30 min deposition of Cs, the central part of the sample, shows Cs clusters with approximately 0.8 monolayer (ML) surface coverage (Fig. 4b). The last part of the sample, with 60 min of Cs deposition, shows a full W(110) surface coverage (Fig. 4c). W(110) atomic steps are not sharp, and Cs clusters start to form a second layer of Cs. This part has approximately 1.2 ML of surface coverage with Cs.

Using the model proposed by Chou et al. [8], the work function of clean W(110) changes from 4.68 eV to approximately 1.4 eV at 0.8 ML of Cs. Whilst when the surface coverage increases to 1.2 ML, the work function increases to approximately 1.8 eV.

The SPELS spectra were obtained on the three surfaces with a primary electron beam energy of 30 V and tip-sample distance of 200 nm. On the clean W(110) side of the sample, both electron energy analysers show a strong peak of elastically scattered electrons (Fig. 5 a,b). Spectrum recorded on the CLAM also exhibits weaker peaks at approximately 6 eV and 22 eV energy that the BBX does not record. Such electron peaks are detected on all the sample regions, i.e. independent of the material

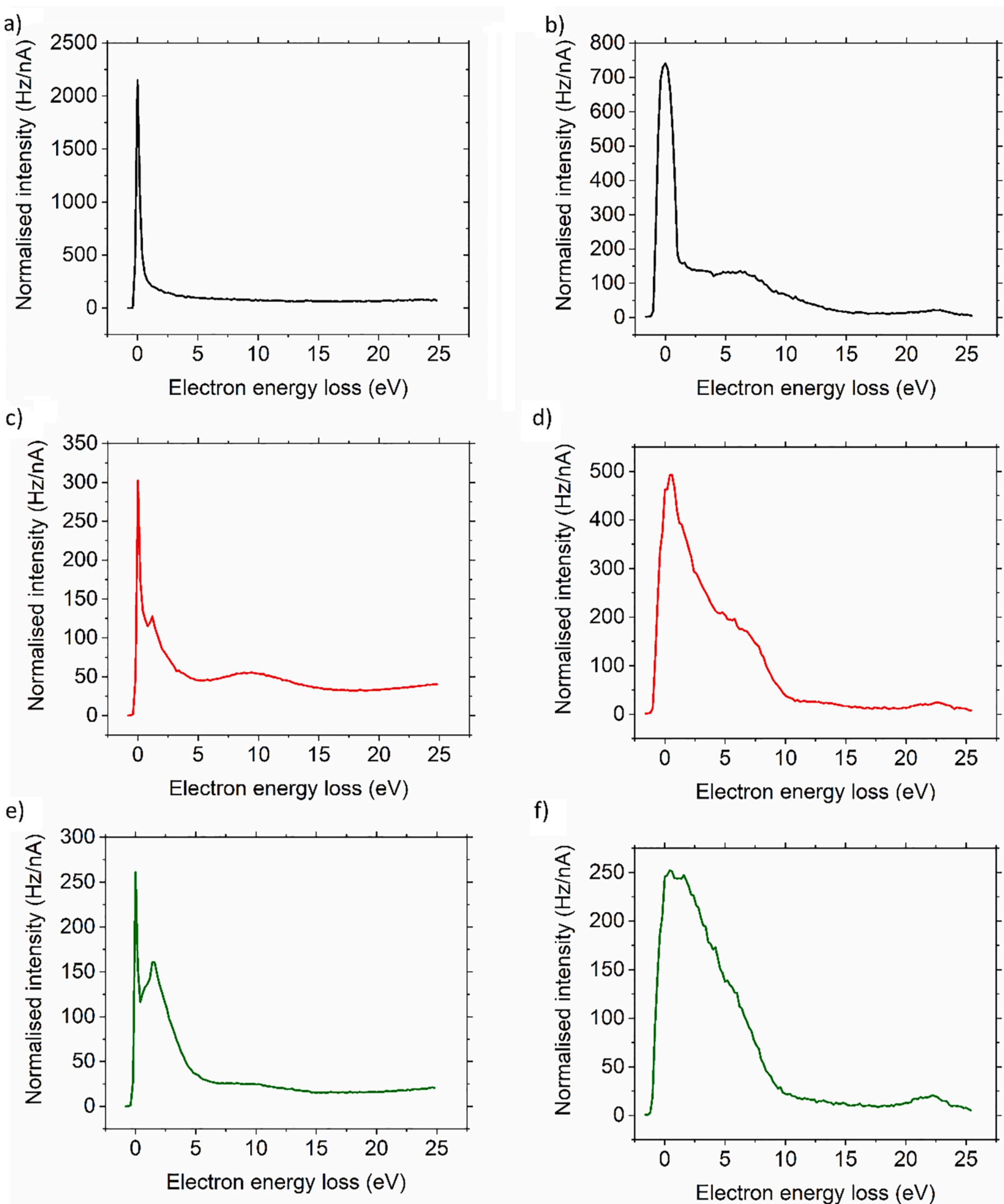

Fig. 5. SPELS spectra of clean W(110) surface detected by a) BBX and b) CLAM detectors, W(110) covered with approximately 0.8 ML of Cs detected by c) BBX and d) CLAM detectors and W(110) covered with approximately 1.2 ML of Cs detected by e) BBX and f) CLAM analysers.

coverage and therefore do not originate from the sample. These two peaks at 6 eV and 22 eV are attributed to internal scattering of electrons in the CLAM [14,15]. Furthermore, we can see that the BBX shows a better energy resolution (marginal difference in the width of the peak of elastically scattered electrons) than CLAM's resolution of 1 eV [16].

Spectra recorded on the surface covered with approximately 0.8 ML of Cs (Fig. 5 c,d) show a more visible difference, than suggested by Werner et al. [5]. On this surface, with smaller work function, electron energy losses are detected with both detectors. First, the absolute intensity of the elastic peak decreased on both detectors. Second, a new peak at ~1.5 eV appears. For the BBX, this peak is distinguishable from the elastic peak whilst for the CLAM, due to its lower resolution, it appears as a shoulder-like feature on the low energy side of the elastic peak.

In the case of a surface fully covered with Cs, the ~1.5 eV peak in the energy loss spectrum collected with the BBX increases in intensity (Fig. 5 e). This 1.5 eV peak was also observed in classical EELS measurements of Cs, where it was observed at coverages above 0.4 ML [17]. Therefore, this peak can be used as a confirmation of the presence of Cs on the sample surface. Spectrum measured with the CLAM (Fig. 5 f) cannot clearly distinguish between elastically scattered electrons and the Cs peak at low energy loss because of its low resolution. Note, however, that the elastic peak width in this case increases to almost twice its width obtained on the clean W(110) surface. This indicates a convolution with the low energy Cs peak, which is now stronger (i.e. more intense) than its value at 0.8 ML coverage. On both electron energy analysers we observed further decrease in the elastic peak intensity with increased coverage of Cs.

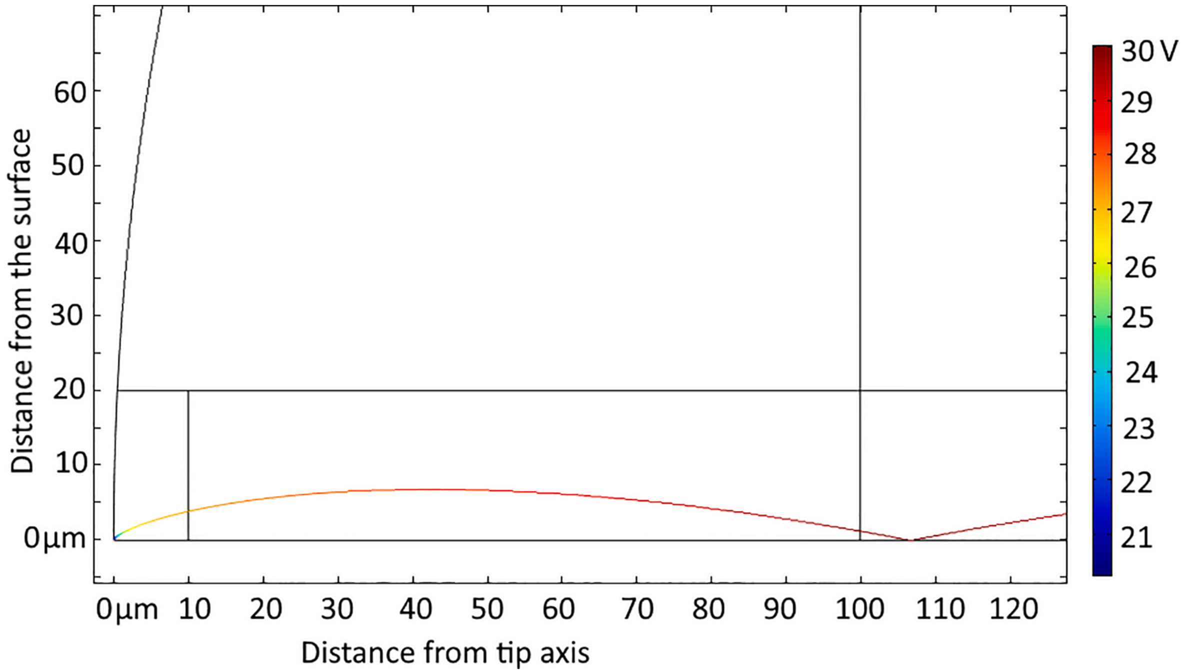

Fig. 6. Electrons launched from under the tip with 30 eV energy and at 20° to the tip axis. Electron trajectory colour coded according to electron kinetic energy.

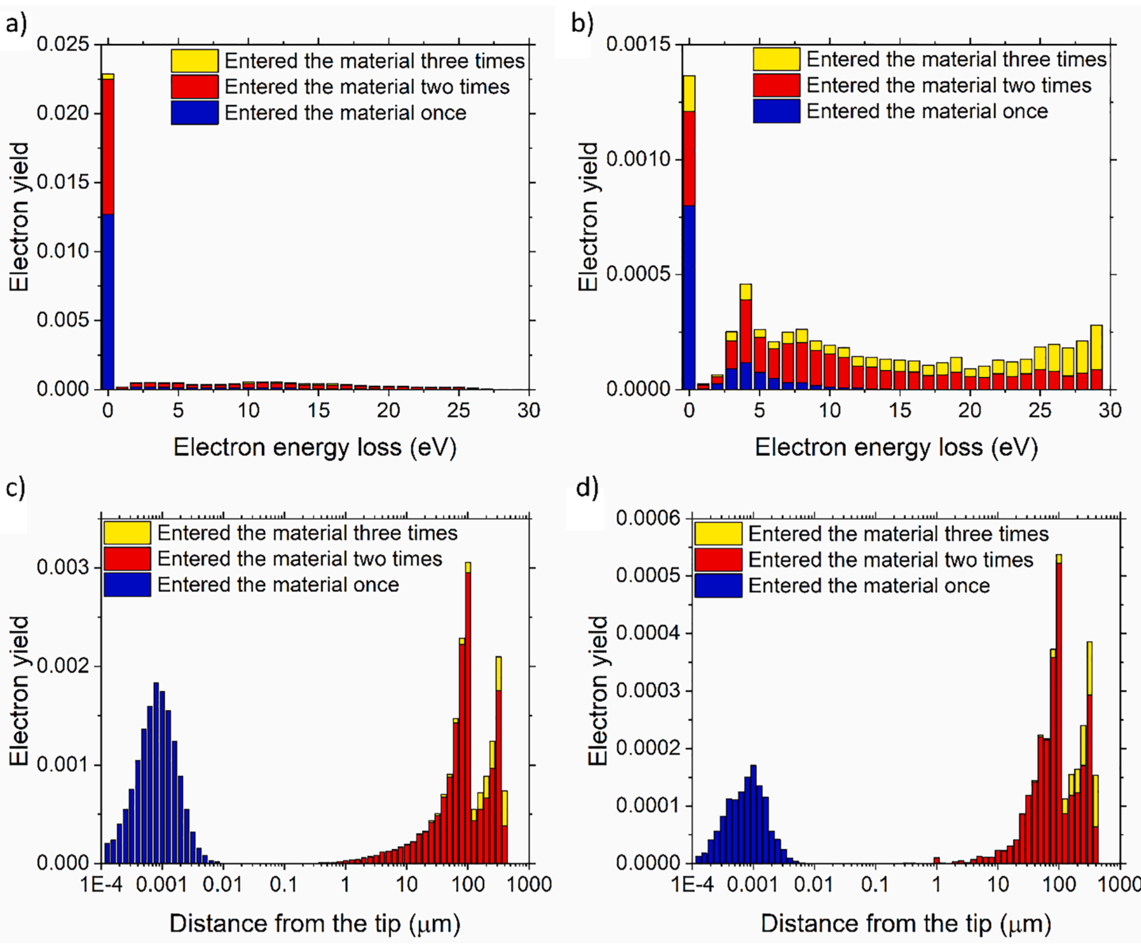

Fig. 7. Simulated spectra acquired from the SFEM and the corresponding origin of the electrons on a) clean W surface and b) 1 ML of Cs on W. The radial distance from the initial electron impact spot at which the electron left the surface of the sample and struck the detector for c) clean W surface and d) 1 ML of Cs on W.

When comparing measured spectra on the BBX and the CLAM, there are two main differences. First is the energy resolution, which is better (higher) for the BBX. Second, the position and number of peaks detected in both detectors are different. Spectra recorded with the BBX show a distinctive peak related to Cs [17], which is indistinguishable in the spectra recorded with the CLAM. On both analysers we can see additional peaks that cannot be attributed to the material-related features and are most likely caused by internal scattering of electrons within the detector.

From experimentally observed spectra, the difference between surfaces with different work functions is noticeable. With the increased surface coverage of Cs, the absolute intensity of elastically scattered electrons decreases, and the intensity of Cs-related [17] low-energy loss peak (~1.5 eV) increases. Such changes observed on both electron energy analysers clearly show that the contribution of the sample's work function is an important parameter, and a novel model of electron-solid interaction in this experimental set-up is required. Unlike the model by Werner et al. [5], we have considered the quantomechanical reflection of electrons from the vacuum/material interface. Allowing the reflection of electrons without energy losses describes the observed results more accurately.

The simulated trajectory of an electron at the primary energy and launched at 20° to the tip axis is shown in Fig 6. At this angle and energy, the electrons travelled distance reaches a maximum of well over 100 μm from the tip-sample junction. At this distant point from the point of primary electron impact, the electron skips one more time before escaping the sample and striking the electron analyser.

Fig. 7 a,b show the simulated spectra from clean W sample and 1 ML of Cs deposited on W(110). Note that the intensity of the elastic peak is much lower after the introduction of Cs, similar to the experimental data. This effect is due to a lower energy barrier for electrons to enter the material, when striking the surface. The probability of an electron to be elastically scattered therefore decreases with increased Cs coverage. The lower intensity of the elastic peak enhances the inelastically scattered electrons, that after introduction of Cs have the intensity in the order of magnitude of elastically scattered electrons. In addition, there is a plasmon loss peak at ~4 eV loss in the simulated spectra for the Cs coated surface. The loss peak is at 1.5 eV in the experiment. The difference can be explained due to the use of bulk dielectric function data in the simulation (i.e. surface plasmons were not simulated). The 4 eV loss-peak, which is attributed to bulk plasmon losses, has also been detected in classical EELS [17], but is much weaker than that of the surface plasmon peak at 1.5 eV and at slightly higher energy of about 5 eV. This peak is likely to be convoluted with the broader internally scattered electrons at 9 eV and with the steep low energy shoulder of the elastic and 1.5 eV peaks. Fig. 7 c, d show the distance from the tip when the electron last left the surface and then struck the detector. If the electron skips quantomechanically, it is assumed not to re-enter the material and will continue to have the properties (e.g. spin) that it adopted when it was previously in the material.

Our simulation model confirms that the lower-energy (i.e. those that appear as high energy loss in the spectra) electrons do not originate from under the tip. The combination of quantomechanical skipping and inelastic scattering of electrons inside the sample allows electrons to be emitted from even several hundreds of micrometres away from the tip. It is not possible to experimentally verify this with standard electron energy analysers (EEAs). Standard EEAs, as in the case of the CLAM used here, are usually bulky, and it is not possible to *in-situ* move them. However, with the BBX, which is small, mobile, and located only millimetres away from the sample, we could experimentally detect spectra from different parts of the sample by *in-situ* moving it over different parts of the sample. By moving BBX while the tip remains at the same spot, we can predominantly collect electrons that originated from well away from the point of primary electron impact. All the above-presented spectra were recorded with BBX located at the position with a maximal intensity of elastically scattered electrons. The BBX was moved parallel to the sample surface (i.e. along x-axis), and three additional spectra were recorded at the surface with a 1.2 ML Cs surface coverage (Fig. 8). Recorded spectra were normalised to the intensity at 1.55 eV energy loss (Cs peak) to visualise the results better. Moving the BBX away from the aligned position results in a fast decrease in the intensity of elastically scattered electrons. After moving 175 μm off the aligned position, the elastic peak is nearly half its original maximum value, i.e. the BBX's field of view is outside the point of electron impact and the area of the emitted electrons as a result of the incident electrons, which is the condition in conventional electron spectroscopy. In contrast, detection of electrons in electron microscopy could include secondary and backscattered electrons as well as tertiary and even quaternary scattered electrons, often from the chamber walls of the experimental set-up. Moving another 100 μm decreases the detected intensity of elastically scattered electrons to the level that the energy resolution barely allows us to distinguish this peak from the low-energy loss electrons. When the BBX has moved in total 475 μm away from the aligned position, the elastic peak is no longer present, and only electrons with low-energy losses are detected. It is noteworthy that these low-energy loss electrons do no longer form an observable peak at this position but only a low-intensity background. This measurement allowed us to distinguish between the electrons originating from under the tip and electrons that emerged from the surface hundreds of microns away from the tip-sample junction, which are due in this set-up to quantomechanical effects, as discussed in this study.

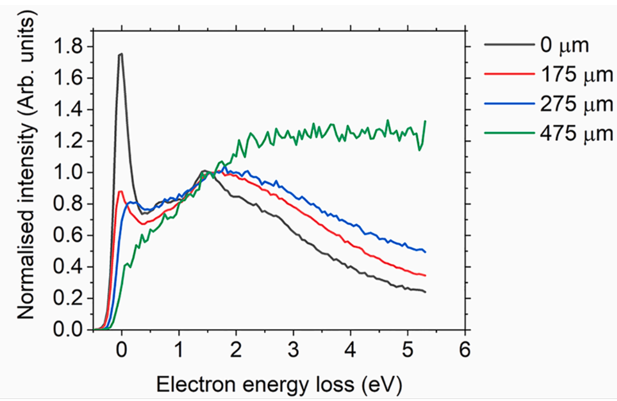

Fig. 8. SPELS spectra detected at different positions of the BBX. All spectra are normalised to have 1 Arb. unit at the 1.5 eV energy loss. The black curve shows the spectrum recorded at the aligned position, where the highest intensity is detected. The red curve shows a spectrum recorded 175 μm away from the alignment position. The blue curve shows a spectrum recorded 275 μm away from the alignment position and the green curve represents a spectrum with the BBX moved 475 μm away from the alignment.

Conclusions

Scanning Field Emission Microscopy has been applied to W(110) and thin films of Cs deposited on W(110) to vary a work function of the sample surface. First, the absolute intensity of the elastically scattered electrons is inversely proportional to the Cs coverage. Second, the Cs-related peak was detected and its intensity was directly proportional to the Cs coverage. Simulations of the experiments using a combination of finite element modelling of the trajectories in the vacuum and Monte Carlo modelling of the trajectories in the material show good agreement with the experimental results. The results are strongly influenced by electrons skipping off the surface due to a quantomechanical effect. In addition, some electrons emerge from under the tip-sample junction, but others emerge from the surface up to several hundred microns away from the tip-sample junction. With the use of a miniature electron energy analyser, the electrons that emerge from the tip-sample junction can be preferentially detected.

Therefore, for SPELS operated in the field emission regime, the proximity and the field of view of the detector play a major role on the quality of spectra. With such a miniature and mobile detector as the BBX, spectral features of individual materials can be distinguished even with the tip in a close proximity to the sample.

Finally, the experimental set-up described above of a SFEM together with a miniature electron energy analyser pave the way to achieve SPELS at high spatial resolution approaching one nm, as has been previously demonstrated with SFEM [1].

Declaration of Competing Interest

The authors declare that they have no known competing financial interests or personal relationships that could have appeared to influence the work reported in this paper.

Acknowledgments

The authors would like to thank COMSOL Multiphysics Support for all their assistance in the simulation aspect of this work. The ISG group at ETH Zürich provided help in setting up the Geant4 package. Financial support by the FP7 People: Marie-Curie Actions Initial Training Network (ITN) SIMDALEE2 (Grant No. PITN 606988) is gratefully acknowledged.

References

[1] D.A. Zanin, L.G. De Pietro, Q. Peter, A. Kostanyan, H. Cabrera, A. Vindigni, T. Bähler, D. Pescia, U. Ramsperger, Thirty per cent contrast in secondary-electron imaging by scanning field-emission microscopy, Proc. R. Soc. A Math. Phys. Eng. Sci. 472 (2016), https://doi.org/10.1098/rspa.2016.0475.

[2] R.E. Palmer, B.J. Eves, F. Festy, K. Svensson, Scanning probe energy loss spectroscopy, Surf. Sci. 502–503 (2002) 224–231, https://doi.org/10.1016/S0039-6028(01)01949-5.

[3] F. Festy, R.E. Palmer, Scanning probe energy loss spectroscopy below 50 nm resolution, Appl. Phys. Lett. 85 (2004) 5034–5036, https://doi.org/10.1063/1.1818742.

[4] B.J. Eves, F. Festy, K. Svensson, R.E. Palmer, Scanning probe energy loss spectroscopy: Angular resolved measurements on silicon and graphite surfaces, Appl. Phys. Lett. 77 (2000) 4223–4225, https://doi.org/10.1063/1.1333404.

[5] W.S.M. Werner, M. Oral, T. Radlička, J. Zelinka, I. Müllerová, A. Bellissimo, G. Bertolini, H. Cabrera, O. Gürlü, Scanning tunneling microscopy in the field-emission regime: Formation of a two-dimensional electron cascade, Appl. Phys. Lett. 115 (2019), 251604, https://doi.org/10.1063/1.5128300.

[6] M. Hirade, T. Arai, M. Tomitori, Detection improvement for electron energy spectra for surface analysis using a field emission scanning tunneling microscope, Japanese J. Appl. Physics, Part 1 Regul. Pap. Short Notes Rev. Pap. 42 (2003) 4837–4840, https://doi.org/10.1143/jjap.42.4837.

[7] A.-K. Thamm, J. Wei, J. Zhou, C.G.H. Walker, H. Cabrera, M. Demydenko, D. Pescia, U. Ramsperger, A. Suri, A. Pratt, S.P. Tear, M.M. El-Gomati, Hallmark of quantum skipping in energy filtered lensless scanning electron microscopy, Appl. Phys. Lett. 120 (2022), 052403, https://doi.org/10.1063/5.0077503.

[8] S.H. Chou, J. Voss, I. Bargatin, A. Vojvodic, R.T. Howe, F. Abild-Pedersen, An orbital-overlap model for minimal work functions of cesiated metal surfaces, J. Phys. Condens. Matter. 24 (2012), 445007, https://doi.org/10.1088/0953-8984/24/44/445007.

[9] A. Suri, A. Pratt, S. Tear, C. Walker, C. Kincal, U. Kamber, O. Gurlu, M. El-Gomati, Analysis and detection of low-energy electrons in scanning electron microscopes using a Bessel box electron energy analyser, J. Electron Spectros. Relat. Phenomena. 241 (2020), 146823, https://doi.org/10.1016/j.elspec.2019.02.002.

[10] D.A. Zanin, H. Cabrera, L.G. De Pietro, M. Pikulski, M. Goldmann, U. Ramsperger, D. Pescia, J.P. Xanthakis, Fundamental aspects of near-field emission scanning electron microscopy. Advances Imaging Electron Phys., Academic Press Inc., 2012, pp. 227–258, https://doi.org/10.1016/B978-0-12-394396-5.00005-1.

[11] S. Agostinelli, J. Allison, K. Amako, J. Apostolakis, H. Araujo, P. Arce, M. Asai, D. Axen, S. Banerjee, G. Barrand, F. Behner, L. Bellagamba, J. Boudreau, L. Broglia, A. Brunengo, H. Burkhardt, S. Chauvie, J. Chuma, R. Chytracek, G. Cooperman, G. Cosmo, P. Degtyarenko, A. Dell'Acqua, G. Depaola, D. Dietrich, R. Enami, A. Feliciello, C. Ferguson, H. Fesefeldt, G. Folger, F. Foppiano, A. Forti, S. Garelli, S. Giani, R. Giannitrapani, D. Gibin, J.J. Gomez Cadenas, I. Gonzalez, G. Gracia Abril, G. Greeniaus, W. Greiner, V. Grichine, A. Grossheim, S. Guatelli, P. Gumplinger, R. Hamatsu, K. Hashimoto, H. Hasui, A. Heikkinen, A. Howard, V. Ivanchenko, A. Johnson, F.W. Jones, J. Kallenbach, N. Kanaya, M. Kawabata, Y. Kawabata, M. Kawaguti, S. Kelner, P. Kent, A. Kimura, T. Kodama, R. Kokoulin, M. Kossov, H. Kurashige, E. Lamanna, T. Lampen, V. Lara, V. Lefebure, F. Lei, M. Liendl, W. Lockman, F. Longo, S. Magni, M. Maire, E. Medernach, K. Minamimoto, P. Mora de Freitas, Y. Morita, K. Murakami, M. Nagamatu, R. Nartallo, P. Nieminen, T. Nishimura, K. Ohtsubo, M. Okamura, S. O'Neale, Y. Oohata, K. Paech, J. Perl, A. Pfeiffer, M.G. Pia, F. Ranjard, A. Rybin, S. Sadilov, E. di Salvo, G. Santin, T. Sasaki, N. Savvas, Y. Sawada, S. Scherer, S. Sei, V. Sirotenko, D. Smith, N. Starkov, H. Stoecker, J. Sulkimo, M. Takahata, S. Tanaka, E. Tcherniaev, E. Safai Tehrani, M. Tropeano, P. Truscott, H. Uno, L. Urban, P. Urban, M. Verderi, A. Walkden, W. Wander, H. Weber, J.P. Wellisch, T. Wenaus, D.C. Williams, D. Wright, T. Yamada, H. Yoshida, D. Zschiesche, GEANT4 - A simulation toolkit, Nucl. Instrum. Methods Phys. Res. Sect. A Accel. Spectrometers, Detect. Assoc. Equip. 506 (2003) 250–303, https://doi.org/10.1016/S0168-9002(03)01368-8.

[12] E. Kieft, E. Bosch, Refinement of Monte Carlo simulations of electron-specimen interaction in low-voltage SEM, J. Phys. D. Appl. Phys. 41 (2008), 215310, https://doi.org/10.1088/0022-3727/41/21/215310.

[13] J. Cazaux, Reflectivity of very low energy electrons (< 10 eV) from solid surfaces: physical and instrumental aspects, J. Appl. Phys. 111 (2012) 64903, https://doi.org/10.1063/1.3691956.

[14] M.M. El Gomati, T.A. El Bakush, Sources of internal scattering of electrons in a Cylindrical Mirror Analyser (CMA), Surf. Interface Anal. 24 (1996) 152–162, https://doi.org/10.1002/(SICI)1096-9918(199603)24:3<152::AID-SIA96>3.0.CO;2-J.

[15] M.P. Seah, Scattering in electron spectrometers, diagnosis and avoidance. I. Concentric hemispherical analysers, Surf. Interface Anal. 20 (1993) 865–875, https://doi.org/10.1002/sia.740201102.

[16] G. Bertolini, Spectro-microscopy in the field emission regime of scanning tunneling microscopy, ETH Zurich (2020), https://doi.org/10.3929/ethz-b-000476660.

[17] J.A.D. Matthew, F.P Netzer, G. Astl, EELS of K and Cs on Ag(001): evidence of sudden change in electronic structure with coverage, Surf. Sci. 259 (1991) L757–L762, https://doi.org/10.1016/0039-6028(91)90547-6.